Nucleon Structure from Lattice QCD

Keh-Fei Liu

Dept. of Physics and Astronomy
Univ. of Kentucky, Lexington, KY 40506

Abstract

We report results on the nucleon structure obtained from the lattice quantum chromodynamics calculation. These include the axial, electromagnetic, πNN, and scalar form factors. The calculation is carried out at $\beta = 6$ on a $16^3 \times 24$ lattice with 24 quenched gauge configurations. The chiral limit results are extrapolated from several light quark cases. For the disconnected insertion (sea-quark contribution), we used the stochastic estimation with the Z_2 noise to calculate the diagonal and off-diagonal traces of the inverse matrices with a size of $10^6 \times 10^6$. It is found that the Z_2 noise is the optimal choice and its comparison with the Gaussian noise for our quark matrix is given. For the sea-quark contribution, we report results on the strange and charm condensates in the nucleon and the $\pi N\sigma$ term.

1 Introduction

The Understanding cannot See.
The Senses cannot Think.
By their union only can Knowledge be produced.

— *Immanuel Kant*

Imagination is more important than Knowledge.

— *Albert Einstein*

The above quotes can be used to describe the two well recognized approaches to scientific research — Experimental and Theoretical. Particularly true to the quotes is the field of strong interaction where there has been an intense interplay between theory and experiment. The advent of quantum chromodynamics(QCD), a non-abelian gauge relativistic quantum field theory of quarks and gluons (the constituents of protons and neutrons), in the early seventies has offered the most promising description of strong interaction dynamics and internal structure of hadrons both in logical consistency and in scope[1]. It is widely accepted that it is the correct theory of strong interaction. This acceptance is based on a substantial amount of experimental data accumulated and refined over the last two decades. It is particularly so for the inclusive scattering processes at large momentum transfer where the perturbative QCD is applicable. On the other hand, confirmation of QCD as the fundamental theory of strong interaction has been somewhat hampered by the lack of analytical calculations of the low frequency modes due to the inherent non-perturbative nature of the theory.

The invention of lattice-regularized QCD[2] with Monte Carlo methods[3] holds the promise of circumventing the difficulty of obtaining analytic results via numerical simulation. In the lattice-regularized gauge theory, the continuous space-time is discretized by a

finite lattice with a periodic boundary condition. As a consequence, the infinite dynamic degrees of freedom associated with the space-time is reduced to a finite number which makes numerical analysis feasible. The recent advancement in supercomputer technology and the DOE Grand Challenge Award have made it possible to carry out large scale Monte Carlo simulations to calculate the hadronic structure and interaction in the framework of lattice QCD. This allows us to compare the lattice results with the experimental data in a qualitative and semi-quantitative manner which is very valuable in understanding physics from first principles free from the uncertainty of models.

In the present paper, we shall report results on the study of the nucleon structure which includes the electromagnetic, axial, pseudoscalar, and scalar form factors and compare them with the known experiments. From the pseudoscalar form factor, we extract the pion-nucleon-nucleon form factor. We also report results on the sea-quark contributions with disconnected current insertions. This entails quark-loop calculations involving diagonal and off-diagonal traces of the inverse quark matrices with a dimension $10^6 \times 10^6$. This is carried out with the stochastic estimation algorithm with the Z_2 noise. We show that the Z_2 noise is actually the optimal choice and a direct comparison with the Gaussian noise is given. From this calculation, we obtain the strange and charm quark condensates in the nucleon.

As we shall see the above computer simulation has already been very helpful in bridging between the theory and experiment via *ab initio* calculations and is doing a job better than the models, this third branch of scientific research will only get more mature when both the computer hardware and algorithm improve with time. To put the numerical simulation in perspective, we maintain:

> Imagination may not be relevant.
> Knowledge cannot predict.
> By simulating Imagination and testing against Knowledge
> only can Reality be re-created.

2 Formalism and Numerical Steps

The Euclidean path integral formulation of quantum field theory is employed to calculate the Green's function. In this way, the quantum field theory becomes a problem in classical statistical mechanics. Physical observables are then extracted from the statistical correlation functions of composite operators built on the fundamental dynamical variables in quark and gluon fields. In the following, we present a synopsis of the formalism and related numerical steps.

The correlation functions have the following generic form

$$< O_1(U,\bar{\psi},\psi)O_2(U,\bar{\psi},\psi)... >= \frac{1}{Z}\int [dU][d\psi][d\bar{\psi}]e^{-S_G-S_F}\bar{\psi}_\alpha\bar{\psi}_\beta...T^{\alpha\beta...}_{\alpha'\beta'...}(U)...\psi_{\alpha'}\psi_{\beta'}..., \tag{1}$$

where Z is the partition function. S_G is the action of the gauge link variable U and S_F the fermion action which is bilinear in the quark field variable ψ and can be written in the form $S_F = \bar{\psi}M[U]\psi$. Since both the fermion action S_F and the operator product $O_1O_2...$ are bilinear in $\bar{\psi}$ and ψ, the fermion integral over the anti-commuting Grassmann variables

$\bar{\psi}$ and ψ can be done analytically to give

$$< O_1(U,\bar{\psi},\psi)O_2(U,\bar{\psi},\psi)... >= \frac{1}{Z}\int [dU]e^{-S_G}\det M[U]Tr[M^{-1}[U]M^{-1}[U]M^{-1}[U]...T]. \tag{2}$$

The path integral in eq.(2) is an ordinary multiple integral over the group manifold, in this case $SU(3)$ group. One might think of approximating the integral by summing over a sufficiently dense set of mesh points, say 4 per variable. However , this "modest" goal is well beyond the capacity of the existing supercomputers: for a (small) 10^4 lattice, it would require a calculation on $4^{320,000} = 10^{192,659}$ points. Instead, one may use the important sampling technique to select a comparatively small subset of gauge configurations $(U_1, U_2, ..., U_N)$ among the "important" ones, such that the probability of occurrence of a given configuration U_i in this ensemble approaches the desired distribution

$$[dU]e^{-S_G}\det M[U], \tag{3}$$

for $N \to \infty$. Then the quantum average are given(for sufficiently large N) by averages taken over the sample: that is

$$< O_1O_2... >= \frac{1}{N}\sum_{i=1}^{N} Tr[M^{-1}[U_i]M^{-1}[U_i]...T] \pm O(\frac{1}{\sqrt{N}}). \tag{4}$$

There are three numerical steps to lattice gauge calculations. The first step is to prepare an ensemble of gluon configurations $\{U_i\}$ in the vacuum. This is done using the Cabibbo-Marinari[4] pseudo-heatbath algorithm, a Monte Carlo method which generates sets of link matrices $\{U_i\}$ according to the distribution in eq.(3). In principle, the probability distribution includes a factor of $\det(M[U])$ which represents the effect of quark-antiquark polarization in the vacuum. In the present simulations, we omit this factor as an approximation since it would require more computation than we can do. We will discuss the validity of this approximation when we come to the results of the calculations. Omitting this determinant is referred to as the quenched approximation.

The second step is to calculate the quark propagator matrix $M^{-1}[U]$ in the prepared gluon (U) background. This is done with the conjugate-gradient algorithm[5]. This is an iterative scheme which is capable of giving the desired solution to arbitrary accuracy. We typically find a few hundred iterations to be sufficient.

The last step is to assemble the quark propagator matrices $M^{-1}[U_i]$ and the the matrix $T[U_i]$ defined in eqs. (1) and (2) to evaluate the correlation function in eq.(4) from which we extract the physical quantities with statistical analysis.

3 Form Factors of Nucleon

3.1 Formalism

Electron and neutrino scatterings off the nucleon target are useful probes of the nucleon internal structure by measuring its electromagnetic and axial form factors. These form factors can be simulated in the lattice gauge calculation and compared with experiments directly and thereby serve as a test to the Monte Carlo calculation and the theory as well.

The πNN coupling form factor is a fundamental quantity in the pion-nucleon and nucleon-nucleon dynamics. Yet it is not experimentally accessible directly and is poorly known theoretically. From the calculation of the pseudoscalar form factor, we extract the πNN form factor with pion pole dominance. In this case, it is a prediction from the fundamental theory and will have great help in settling the large uncertainty over the shape and the cutoff of the πNN form factor. Furthermore, there have been sprouting interest in the sea-quark contributions to the nucleon structure, for example, the $\pi N\sigma$ term, the strange and charm condensates in the nucleon and the flavor-singlet axial charge g_A^1. The recent deep inelastic scattering experiment obtained a very small g_A^1 which suggests that most of the spin of the proton does not come from the quark spin which is a great surprise and has been dubbed the "proton spin crisis". Since no model we know has a handle on this problem, we expect the answer to come from the lattice QCD calculation.

The nucleon can be obtained from the following two- and three-point correlation functions [6, 7, 8]

$$G_{NN}(t,\mathbf{p}) = \sum_{\mathbf{x}} e^{-i\mathbf{p}\cdot\mathbf{x}} < 0|N_\alpha(x)\bar{N}_\alpha(0)|0> . \tag{5}$$

$$G_{NjN}(t_1,t_2,\mathbf{p},\mathbf{q}) = \sum_{\mathbf{x_1},\mathbf{x_2}} e^{i\mathbf{q}\cdot\mathbf{x_1}-i\mathbf{p}\cdot\mathbf{x_2}}\Gamma^{\alpha\beta} < 0|N_\beta(x_2)j_\mu(x_1)\bar{N}_\alpha(0)|0>, \tag{6}$$

where N_α represents the proton or neutron interpolating field with the Dirac component α, Γ is a 4×4 matrix in the Dirac space and j_μ represents various bilinear quark currents in the form of $\bar{\Psi}\Sigma\Psi$. By inserting complete sets of states and setting $t_2 >> t_1 >> a$, the lattice spacing, we obtain the electromagnetic form factors $G_E(q^2)$ and $G_M(q^2)$, axail form factor $g_A(q^2)$, pseudoscalar form factor $g_P(q^2)$, and scalar form factor $g_S(q^2)$ from the ratios of the three point functions involving corresponding currents to two point functions. The results corresponding to the physical quark masses are obtained from the extrapolation from those with heavier quarks to the chiral limit where the pion mass is zero.

3.2 Numerical details

Our results are based on 24 quenched (ignoring the determinant in eq. (3) gauge configurations on a $16^3\times24$ lattice and were calculated using the Monte Carlo Cabibbo-Marinari pseudo-heatbath algorithm[4]. The $SU(3)$ fundamental Wilson action was used with periodic boundary conditions and the coupling constant was set at $\beta = 6.0$. The gauge field was thermalized for 5000 sweeps from a cold start and 24 configurations separated by at least 1000 sweeps were saved. For the quarks we use periodic boundary conditions in the spatial directions and "fixed" time boundary conditions, which corresponds to setting the quark couplings across the time edge to zero. The origin of all quark propagators was chosen to be at lattice time site 5; the secondary zero momentum nucleon source was fixed at time site 20. We expect that these positions are sufficiently far from the lattice time boundaries to avoid nonvacuum contaminations. We used the red-black pre-conditioned conjugate-gradient algorithm for the quark propagator. For our convergence criterion we demanded that the absolute sum of the squares of the quark propagators be less than 5×10^{-5} over 5 iterations. As a check of the nucleon secondary source, we verified current conservation for $t_2 > t_1 > 0$ to $O(10^{-4})$.

3.3 Stochastic Estimation with Z_2 Noise

Our present space-time lattice with merely the size of $16^3 \times 24$ gives a quark matrix of the dimension $10^6 \times 10^6$ including the spin and color degrees of freedom. While it is durable to calculate the quark propagator, i.e. $M^{-1}(x,0)$ for a point source S at 0 with a reasonably small quark mass (e.g. a fraction of the strange quark mass) on today's supercomputers, the quark propagator $M^{-1}(x,y)$ from any point to any point is certainly unattainable. For calculations of the 2-point functions (eq. (5) and 3-point functions (eq. (6) with connected insertions for flavor non-singlet currents, one can get by with the help of translational symmetry and uses only $M^{-1}(x,0)$. But there are cases where one can not rely on such a help. These include the calculations of quark loops which are space-time or space integrations of the fermion propagators. Examples of interest in QCD include the quark condensate and the topological susceptibility with the fermion method, flavor-singlet meson masses which involve disconnected quark loops in the two-point functions, notably the U(1) problem., and the πN σ term and the proton spin problem which involve quark loop contributions in the three-point functions.

Instead of waiting for the advent of more powerful hardware, we have employed the stochastic algorithm with the Z_2 noise to estimate the quark loops [9]. Stochastic approach to estimating the inverse of an $N \times N$ matrix M entails the introduction of an ensemble of L column vectors $\eta \equiv \eta^1, ..., \eta^L$ (each of dimension $N \times 1$) with the properties of a white noise, i.e. $\langle \eta_i \rangle = 0, \langle \eta_i \eta_j \rangle = \delta_{ij}$, The expectation value of the matrix element M^{-1}_{ij} can be obtained by solving for X_i in the matrix equations $MX = \eta$ with the L noise vectors η and then take the ensemble average with the j-th entry of η

$$E[M^{-1}_{ij}] = \langle \eta_j X_i \rangle = \sum_k M^{-1}_{ik} \langle \eta_j \eta_k \rangle = M^{-1}_{ij}. \tag{7}$$

which is the matrix element M^{-1}_{ij} itself. In fact, it has been shown recently [10] that the variance of a inverted matrix element due to the stochastic estimation is composed of two parts

$$Var[M^{-1}_{ij}] = \frac{1}{L}\{[M^{-1}_{ij}]^2 C_2^2 + \sum_{k \neq j} [M^{-1}_{ik}]^2\}. \tag{8}$$

Whereas the second part is independent of the kind of noise used, the first part is proportional to the square of the diagonal error $C_2 = \sqrt{\frac{1}{N}\sum_i (\langle \eta_i \eta_i \rangle - 1)^2}$. Since Z_2, or Z_N for that matter, has no diagonal error, i.e. $C_2 = 0$, it produces a **minimum** variance. Other noises will have larger variances due to the non-vanishing C_2. For example, $C_2 = \sqrt{2/L}$ for the Gaussian noise with large and independent configurations.

The question remains as to whether the Z_2 noise is superior than the other noises on a practical footing with reasonable small L. To answer this question, we have tested the usefulness of the Z_2 noise against the Gaussian noise for small noise configurations L ($L \leq 100$) and smaller quark masses. Plotted in the left column in Fig. 1 are the accumulated averages for the estimate of the real part of the diagonal trace $ReTr \sum_{\vec{x}} M^{-1}(x,x)/V$ as a function of L for the Z_2 and Gaussian noises with Wilson hopping parameters $\kappa = 0.148, 0.152$ and 0.154 for a gauge configuration. With $\kappa_c = 0.1568$, $\kappa = 0.152$ corresponds to the strange quark mass and $\kappa = 0.154$ corresponds to a mass about half of that. The straight line is the result from the stochastic estimate at L = 300. We see that the estimate from the Z_2 noise

approaches the value at L= 300 (assumed to be the asymptotic value) faster than that of the Gaussian noise. The corresponding jackknife errors for different L (the right column in Fig. 1) show that the Z_2 noise is consistently better than the Gaussian noise by a factor of two for all three $\kappa's$. This means that to achieve the same level of accuracy for the diagonal trace, one needs statistics for the Gaussian noise about 4 times as much as for the Z_2 noise. We have also examined the near diagonal trace related to the point-split axial current. The result is similar to that of the diagonal trace [9].

We have employed the Z_2 noise to calculate the quark loops in the presence of the nucleon with L = 200 to 300 only. Some of the results will be reported in the next section. Compared with the brute force approach of inverting the whole quark matrix, we have saved the computer time by as much as a factor of 6000!

It is worthwhile noting that the stochastic estimation is particularly successful for the trace (denotes as $Re\overline{\Psi}\Psi$ in Fig. 1). This is due to the translational, color and spin symmetries. As a result, the error is proportional to $1/\sqrt{N}$ where N is the dimension of the matrix. With $N = 1.18 \times 10^6$ in our case and the ratio $\sum_{k\neq 1}[M^{-1}_{k1}]^2/[M^{-1}_{11}]^2 = 0.8$, we predict the error to signal ratio to be $\sqrt{1.5} \times 10^{-3}$ from eq. (8) for L = 1. This agrees well with the numerical calculation shown in Fig. 1. Given this level of accuracy, it is feasible to apply the stochastic method to the calculation of the determinant, the eigenvalues, and the eigenvectors of the matrix M which might not be feasible with other algorithms.

4 Results

We present our results in three groups. The first group includes the electromagnetic and axial form factors where the experimental results are available. We shall compare them with our calculation directly. The second group consists of the πNN form factor deduced from the pseudoscalar form factor where is no direct experimental result available. The third group involves flavor-singlet quantities which require the quark loop calculation with disconnected insertions like the $\pi N\sigma$, the strange and charm condensates in the nucleon.

4.1 Electromagnetic and axial form factors

In Fig. 2, we plot the isovector axial form factor extrapolated to the chiral limit for the local current (L.C.) and the point-split current (P-S.C.) in comparison with the experimental result. In doing so, we have used the calculated nucleon mass to set the scale for the momentum [8]. In addition, we also show the calculated electric form factor G_E extrapolated to the chiral limit and the corresponding experimental results. The experimental $g_A(q^2)$ has been measured in neutrino-neutron scattering and pion electroproduction. The neutrino data gives a good fit in the dipole form up to $q^2 = 3\text{GeV}^2/c^2$ [11], i.e. $g_A(q^2) = g_A(0)/(1-q^2/M_A^2)^2$, with the axial vector coupling constant $g_A(0) = 1.254 \pm 0.006$ and $M_A = 1.032 \pm 0.036$GeV (world average). The new data from Brookhaven E734 experiment [12] gives a value $M_A = 1.09 \pm 0.03 \pm 0.02$ which is higher than the previous world average. Our fit of the axial form factor to the dipole form yields $M_A = 1.09 \pm 0.05$GeV for the P-S.C. and $M_A = 1.06 \pm 0.04$GeV for the L.C. which are closer to the new experimental fit of the Brookhaven E734 data [12]. Similarly, the fitted dipole mass for G_E is $M_E = 0.857 \pm 0.036$GeV which is close to the experimental dipole mass of 0.828 ± 0.006GeV [13]. Comparing to the experimental value $g_A = 1.254(6)$, we find that

the calculated $g_A = 1.20(11)$ and $1.18(11)$ from the P-S.C. and L.C. are 4% and 6% smaller respectively.

4.2 πNN form factor and the induced pseudoscalar form factor

The πNN form factor $g_{\pi NN}(q^2)$ is a fundamental quantity in the low-energy pion-nucleon and nucleon-nucleon dynamics. Many dynamical issues like the πN elastic and inelastic scattering, NN potential, three -body force (triton and He^3 binding energies), pion photoproduction and electroproduction all depend on it. Similarly, the pseudoscalar form factor is important to testing low-energy theorems, chiral Ward identity and the understanding of the explicit breaking of the chiral symmetry. Yet, compared with the electromagnetic form factors and the isovector axial form factor of the nucleon shown in the last section, the pseudoscalar form factor $g_P(q^2)$ and the πNN form factor $g_{\pi NN}(q^2)$ are poorly known either experimentally or theoretically. Notwithstanding decades of interest and numerous work, the shape and slope of $g_{\pi NN}(q^2)$ remain illusive and unsettling. Upon parametrizing $g_{\pi NN}(q^2)$ in the monopole form or the dipole form, the cutoff mass can differ as much as a factor of 3 in different models.

The πNN form factor (shown in Fig. 3) is obtained from the pseudoscalar form factor with pion pole dominance [14]. We fitted it with both a monopole form and a dipole form. We found that the monopole form with $\Lambda_{\pi NN} = 0.75 \pm 0.14$GeV agrees with the Goldberger-Treiman relation at $q^2 = 0$ and the dipole form does not. Extrapolation of the monopole fit to $q^2 = m_\pi^2$ gives $g_{\pi NN} = 12.7 \pm 2.4$ which agrees well with the phenomenological value of 13.40 ± 0.17. $g_{\pi NN}(0) = 12.2 \pm 2.3$ which agrees with the GT relation.

This is a good example where the important physical quantity is not directly accessible experimentally or reliably obtainable from the models, lattice calculation can fill the void and give a reliable prediction.

4.3 $\bar{s}s$ and $\bar{c}c$ in the nucleon and $\pi N\sigma$ term

The matrix element elements $\langle N|\bar{s}s|N\rangle$, $\langle N|\bar{c}c|N\rangle$, and the $\pi N\sigma$ term requires the quark loop calculation with disconnected insertions.

For the disconnected insertion of the current $J(\vec{x},\tau) = \overline{\Psi}(\vec{x},\tau)\Gamma\Psi(\vec{x},\tau)$, we calculate the ratio of the three- and two-point functions.

$$\frac{\langle N(t)\sum_{\tau,\vec{x}} J(\vec{x},\tau)N^\dagger(0)\rangle}{\langle N(t)N^\dagger(0)\rangle} - \sum_{\tau,\vec{x}}\langle J(\vec{x},\tau)\rangle \longrightarrow_{t>>a} const + t\langle N|\overline{\Psi}\Gamma\Psi|N\rangle_{dis}. \qquad (9)$$

Here N is the nucleon interpolation field and $\vec{x}$ is summed over to obtain the forward matrix element. Hence, the matrix element can be obtained as the slope from the above ratio. Since we use the fixed boundary condition for the quark field in the time direction, τ is summed to 4 steps away from the time-boundary in both ends to avoid the boundary effect.

Plotted in Fig. 4 are the ratios defined in eq. (9) for quark masses ranging from the charm (Wilson $\kappa = 0.120$) to strange ($\kappa = 0.154$). We see clearly that the slope becomes larger when the quark mass becomes smaller. Extrapolating to the chiral limit, we obtain

$\langle N|\bar{u}u + \bar{d}d|N\rangle_{dis} = 1.34(26)$ as the lattice renormalized matrix element. This is quite large, about half of the connected insertion $\langle N|\bar{u}u + \bar{d}d|N\rangle_{con} = 2.86(6)$. If we take the renormalized quark mass to be 7 MeV, the calculated $\pi N\sigma$ term is then 29.4 ± 1.9 MeV. This is still smaller than the 45 MeV obtained from πN scattering but is already 50% larger than that secured from the connected insertion alone or equivalently from the derivative of the nucleon mass with respect to the quark mass.

We have also calculated $\langle N|\bar{s}s|N\rangle$ and $\langle N|\bar{c}c|N\rangle$. In this case, the quark mass in the loop due to the current self-contraction corresponds to the strange ($\kappa = 0.154$) and charm ($\kappa = 0.120$). The valence quarks in the nucleon interpolating filed are then extrapolated to the chiral limit. For the strange condensate, we obtain $\langle N|\bar{s}s|N\rangle = 0.43 \pm 0.07$. If the strange quark mass is taken to be 130 MeV, then the strange will contribute $\sim 56 \pm 9$ MeV to the nucleon mass. For the charm case, we obtain $\langle N|\bar{c}c|N\rangle = 0.048 \pm 0.016$. Given the charm mass at 1.3 GeV, it shows the charm can contribute as large as 64 ± 21 MeV to the nucleon mass.

5 Computational Aspects and Conclusion

We have demonstrated in this paper that it is feasible to perform *ab initio* calculations of the hadronic structure directly from the fundamental field theory—quantum chromodynamics without having to rely on models. Notwithstanding the fact that the present lattice size is modest (e.g. $16^3 \times 24$), the quark masses used are heavy compared to the physical situation, the quenched approximation is used, and the Z_2 noise algorithm saved us 6000 times of the computer time for the quark loop calculation, present calculations still took substantial supercomputer resources to perform. For example, the project on the quark loop calculation took 2000 C-90 CPU hours at 1 GFLOP/processor speed to accomplish. For the $16^3 \times 24$ lattice, the memory requirement is 20 Megawords.

In order to test QCD as the fundamental theory and make predictions to compare with experiments beyond doubt, we need to push the calculation to a much larger lattice, a smaller quark mass and with the full description of the dynamic fermions (non-quenched approximation). Each of these directions will demand one or more orders of magnitude in speed and memory than the present calculation requires.

This work is partially supported by DOE Grant DE-FG05-84ER40154. The author is indebted to S.J. Dong, T. Draper, W. Wilcox, and C.M. Wu who collaborated on the projects presented here. He is grateful to DOE for the generous Grand Challenge Award which makes the calculations possible.

References

[1] G. 't Hooft, Proc. of the European Physical Society: International Conference on High Energy Physics, Lisbon(1981).

[2] K.G. Wilson, Phys. Rev. **D10**, 2445(1974).

[3] M. Creutz, L. Jacobs, and C. Rebbi, Phys. Rev. Lett. **42**, 1390(1979) ; Phys. Rev. **D20**, 1915(1979).

[4] N. Cabibbo and E. Marinari, Phys. Lett. **119B**, 387(1982).

[5] M.R. Hestenes and E. Stiefel, Jour. Res., NBS**49**, 409(1952).

[6] T. Draper, R.M. Woloshyn and K.F. Liu, Phys. Lett. **234B**, 121 (1990).

[7] W. Wilcox, T. Draper, and K.F. Liu, Phys. Rev. **D 46**, 1109 (1992).

[8] K.F. Liu, S.J. Dong, T. Draper, J.M. Wu, and W. Wilcox, Phys. Rev. **D 49**, 4755 (1994).

[9] S.J. Dong and K.F. Liu, Nucl. Phys. **B26**(Proc. Suppl.), 353 (1992); Phys. Lett. **B328**, 130 (1994).

[10] S. Bernardson, P. McCarty, and C. Thron, Comp. Phys. Communications, **78**, 256 (1994).

[11] N. Baker *et al.*, Phys. Rev. **D23**, 2499 (1981); K. Miller *et al.*, Phys. Rev. **D26**, 537 (1982); T. Kitagaki *et al.* Phys. Rev. **D28**, 436 (1983).

[12] L.A. Ahrens, Phys. Lett. **B202**, 284 (1988).

[13] G.G. Simon et al., Z. Naturforsch. **35a**, 1 (1980).

[14] K.F. Liu, S.J. Dong, T. Draper, and W. Wilcox, submitted to Phys. Rev. D.

Figure Caption

Fig. 1 The accumulated averages of the real part of the diagonal trace as estimated by the Z_2 and Gaussian noises for three quark masses as functions of L, the number of noise vectors, are plotted in the left column. The right column shows the corresponding jackknife errors as functions of L.

Fig. 2 The calculated axial form factor $g_A(q^2)$ and the proton electric form factor $G_E(q^2)$ as a function of the momentum transfer $-q^2$. The solid and the dash-dotted lines are fit to two experimental sets of data with different dipole masses. The dashed curve is the fit to the experimental $G_E(q^2)$ with a dipole mass of 0.828 GeV.

Fig. 3 The πNN form factor $g_{\pi NN}(q^2)$ at the quark mass which corresponds to the physical pion mass. The solid/dashed line represents the monopole/dipole fit.

Fig. 4 The ratio in eq. (9) for the scalar charge as a function of t for various quark masses. The slope is denoted by M and the χ^2 per degree of freedom is also given.

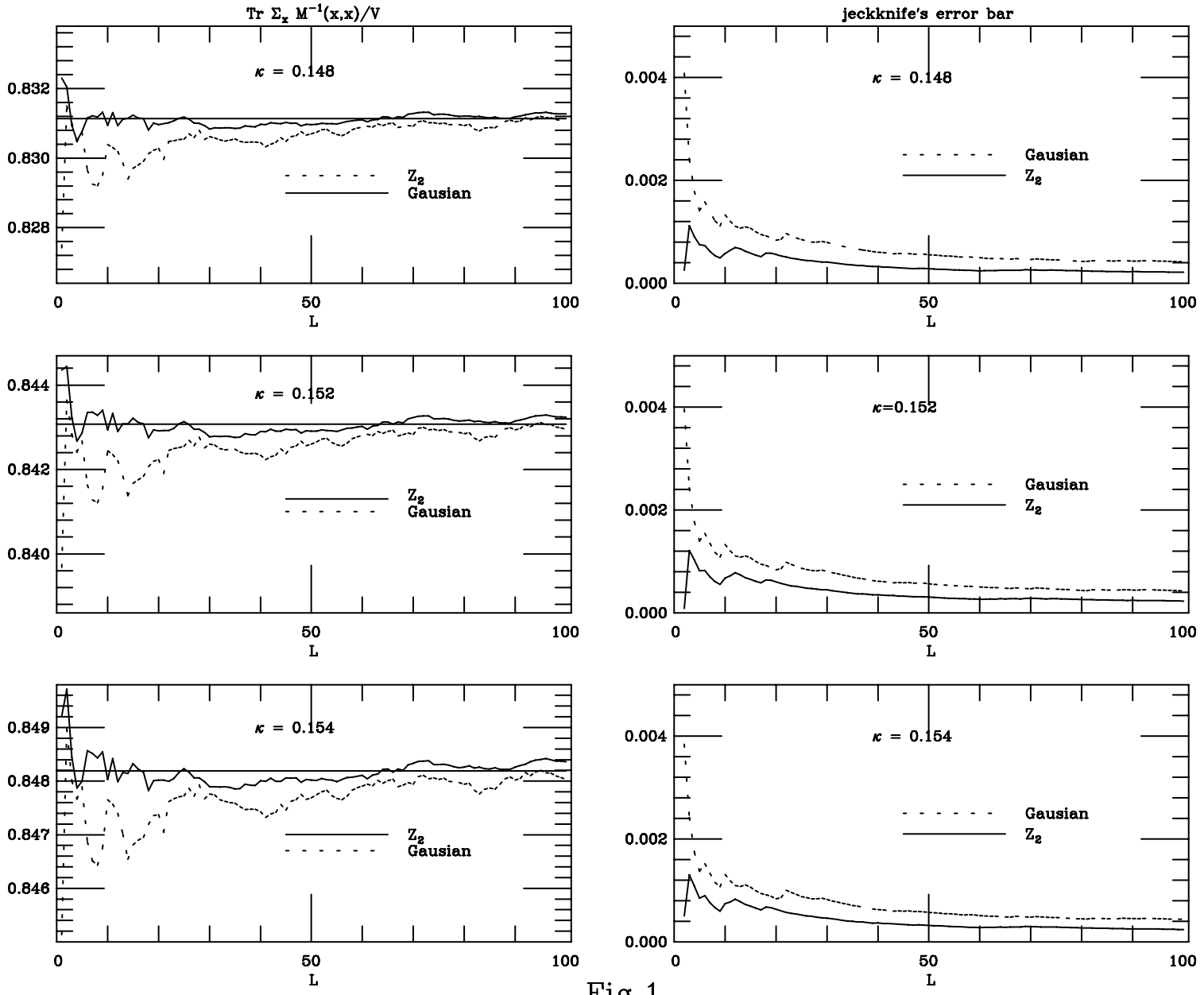
Tr Σ_x $M^{-1}(x,x)/V$
jeckknife's error bar
κ = 0.148
κ = 0.152
κ = 0.154
Z_2
Gausian
L

Fig.1

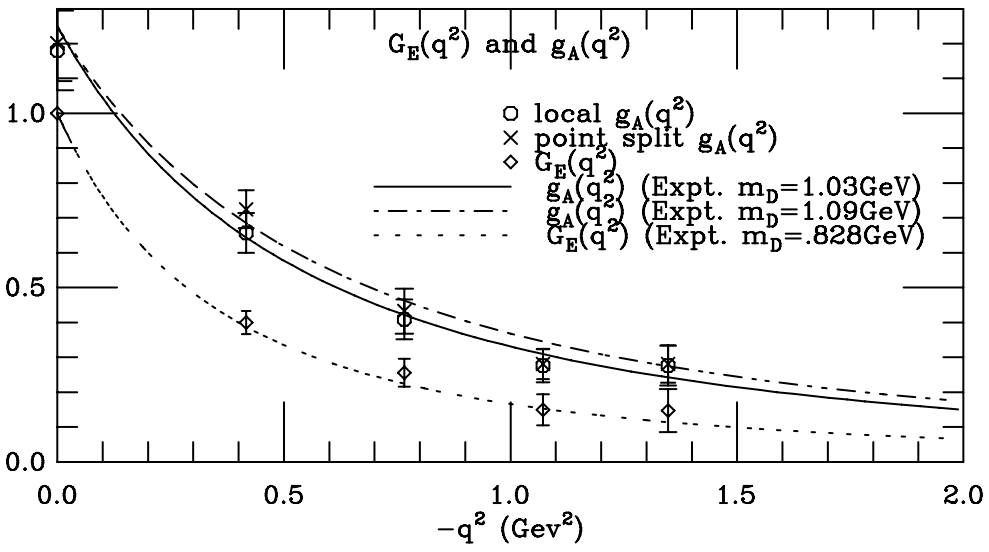
$G_E(q^2)$ and $g_A(q^2)$
local $g_A(q^2)$
point split $g_A(q^2)$
$G_E(q^2)$
$g_A(q^2)$ (Expt. m_D=1.03GeV)
$g_A(q^2)$ (Expt. m_D=1.09GeV)
$G_E(q^2)$ (Expt. m_D=.828GeV)
$-q^2$ (Gev^2)

Fig.2

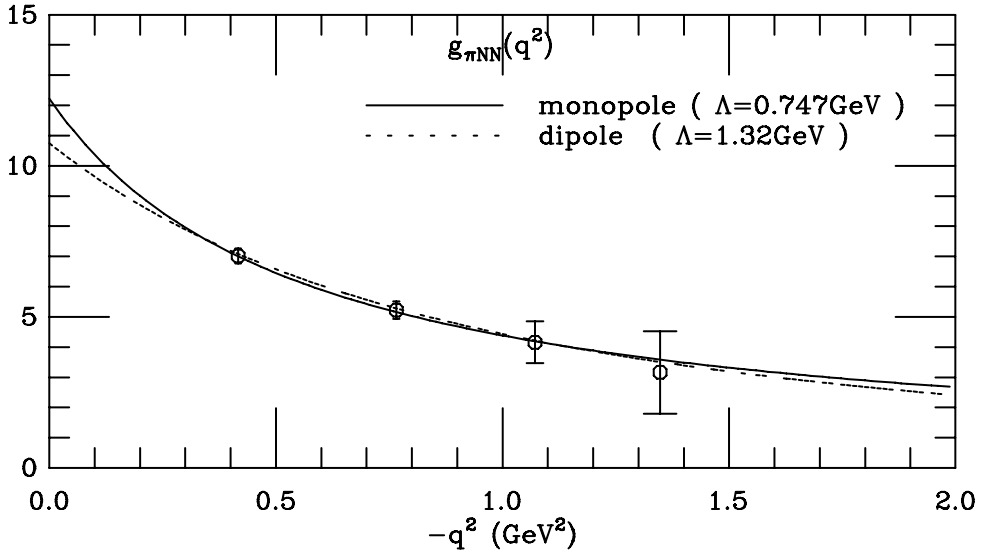
$g_{\pi NN}(q^2)$
monopole (Λ=0.747GeV)
dipole (Λ=1.32GeV)
$-q^2$ (GeV^2)

Fig.3

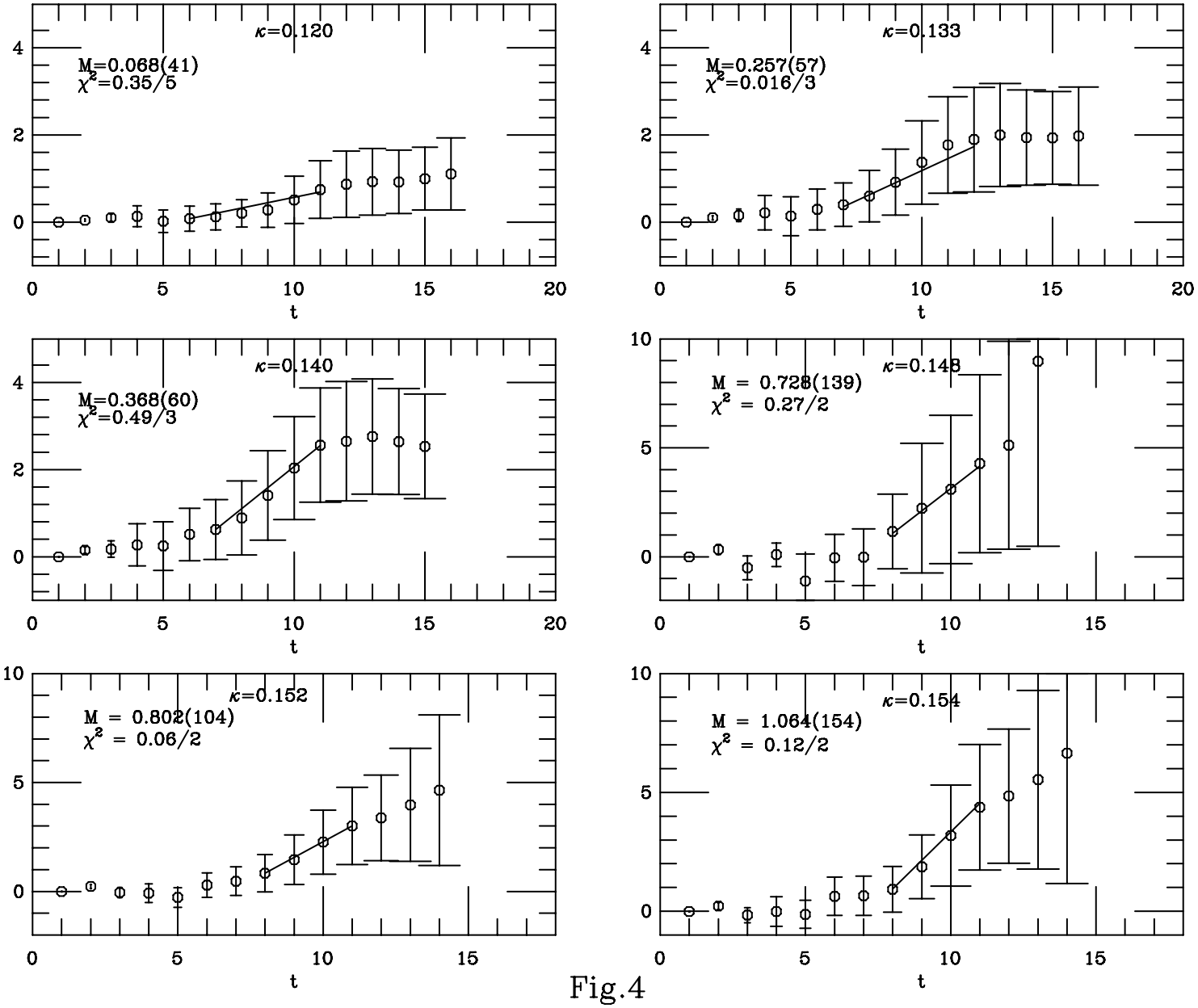
κ=0.120
M=0.068(41)
χ²=0.35/5
κ=0.133
M=0.257(57)
χ²=0.016/3
κ=0.140
M=0.368(60)
χ²=0.49/3
κ=0.148
M = 0.728(139)
χ² = 0.27/2
κ=0.152
M = 0.802(104)
χ² = 0.06/2
κ=0.154
M = 1.064(154)
χ² = 0.12/2
t

Fig.4